Eur. Phys. J. B **59**, 1–8 (2007)
DOI: 10.1140/epjb/e2007-00263-7

THE EUROPEAN PHYSICAL JOURNAL B

Electronic structure and the site preference of manganese in Fe_3Si alloy

A. Go[1,a], M. Pugaczowa-Michalska[2], and L. Dobrzyński[1,3]

[1] Institute of Experimental Physics, University of Bialystok, ul. Lipowa 41, 15-424 Białystok, Poland
[2] Institute of Molecular Physics, Polish Academy of Science, ul. Smoluchowskiego 17, 60-179 Poznań, Poland
[3] The Soltan Institute for Nuclear Studies, 05-400 Otwock-Świerk, Poland

Received 12 March 2007 / Received in final form 24 July 2007
Published online 5 October 2007 – © EDP Sciences, Società Italiana di Fisica, Springer-Verlag 2007

Abstract. Ab initio calculations of the magnetic properties and site preference of Mn in $Fe_{3-x}Mn_xSi$ were carried out using density functional theory and employing the TB-LMTO-ASA method. Qualitative agreement with the experimental results is obtained for site preference as well as for total and local magnetic moments. It is postulated that short-range order would explain observed discrepancies between theoretical and experimental results.

PACS. 71.20.Be Transition metals and alloys – 75.50.Bb Fe and its alloys – 71.20.Lp Intermetallic compounds

1 Introduction

Doped Heusler compounds $Fe_{3-x}Mn_xSi$ with varying Mn content have been investigated experimentally and theoretically. Unusual magnetic and thermal properties of Fe_3Si with Mn substituted for Fe were studied in [1–6]. In addition, the interest in $Fe_{3-x}Mn_xSi$ with low Mn content, $x = 0.05$, was connected with its potential use as an efficient neutron polarizer [7].

The parent Fe_3Si crystallises in the DO_3-type structure. This structure can be described as consisting of four interpenetrating *fcc* Bravais lattices shifted along the body diagonal, originating at $(0,0,0)$, $(\frac{1}{4},\frac{1}{4},\frac{1}{4})$, $(\frac{1}{2},\frac{1}{2},\frac{1}{2})$ and $(\frac{3}{4},\frac{3}{4},\frac{3}{4})$ positions and abbreviated A, B, C and D, respectively. In the perfectly ordered structure iron atoms occupy A, B and C positions whereas silicon atoms are located at D sites. From the crystallographic point of view there are two non-equivalent iron sites. A and C positions are surrounded by four Fe and four Si atoms in the first coordination sphere and are crystallographically equivalent. Eight iron atoms in the nearest neighbourhood surround site B.

In the stoichiometric compound Mössbauer spectroscopy indicates, that small amount of disorder is present between B and D sites [1,2]. It means that some silicon atoms occupy B sites. Nevertheless, this structure combined with an experimental finding of the preferential occupation of sites by transition metal atoms [8–10], makes it extremely useful for studying conditions of magnetic moment formation, as well as the dependence of these moments on the local environment. In particular it was found experimentally that manganese atoms preferentially occupy B positions up to a concentration of $x = 0.75$. Above this concentration Mn atoms also occupy (A,C) sites [9,11,12]. Moreover, Mössbauer measurements indicated partial disorder between (A,C) and D sites while doping with manganese atoms [13]. In other words, some silicon atoms are located at (A,C) positions and, consistently, some Fe atoms occupy D sites.

Fe_3Si is a ferromagnet with a Curie temperature above 800 K [3,9,14]. Different electronic and magnetic properties are connected with two non-equivalent iron positions. In Fe_3Si compound, magnetic moment of iron at B position is reported to be within the range of $2.20\mu_B$ [15] to $2.44\mu_B$ [14]. This value is close to the magnetic moment of iron found in *bcc* structure ($2.2\mu_B$ [16]). This is not unexpected because the nearest neighbourhood of the central iron atom at a B position is the same as for the *bcc* Fe structure. Since the iron atom at an (A,C) site has fewer Fe nearest neighbour atoms, its magnetic moment is smaller too, and within the range of $1.18\mu_B$ [14] to $1.35\mu_B$ [15]. Silicon exhibits a small negative moment arising due to the polarization of conduction electrons [4]. Substitution of iron by manganese atoms causes a decrease of the average magnetic moment and Curie temperature T_C [11]. With a small addition of Mn [17] the decrease of the average magnetic moment was explained within the framework of a band structure model. However no systematic investigation was carried out to determine the moment dependence on manganese concentration. Experimentally it is observed that compounds with the

[a] e-mail: annago@alpha.uwb.edu.pl

concentration below $x = 0.75$ remain ferromagnetic. Further doping with manganese leads to complex magnetic behaviour. Mn_3Si is a non-collinear antiferromagnet [18] with the Neel temperature 25.8 K. Therefore competing interactions arise at higher Mn concentration. Thermal expansion studies of $Fe_{3-x}Mn_xSi$ for $x = 1.2$, 1.5 and 1.8 [5] have shown a decrease with x of the itinerant ferromagnetic character of this alloy. The coefficient of the linear temperature-dependent specific heat obtained from the Stoner-Wohlfarth model, has found to increase with concentration of Mn. The magnon contribution to thermal expansion shows a decrease with Mn addition whereas the magnon part of the entropy increases, thus indicating an increase of the magnetic disorder corresponding to the localised moments [5]. This can be attributed to the antiferromagnetic Mn-Mn interaction, which increases with Mn concentration [5].

This paper presents results of the calculations of the electronic structure of $Fe_{3-x}Mn_xSi$ compound in a range of $0 \leq x \leq 0.5$. A first-principles examination of this system using a supercell approach has been employed to analyse the site preference of manganese atoms and to describe local magnetic properties of constituent atoms. An influence of the local environment on local magnetic moments is discussed in detail.

2 Calculation details

The electronic structure of $Fe_{3-x}Mn_xSi$ has been studied within the framework of the local spin-density approximation, using the self-consistent spin-polarized tight-binding linear muffin-tin orbital method [19] in the atomic sphere approximation (ASA). The exchange correlation potential was taken in the form of von Barth and Hedin [20]. The Langreth-Mehl-Hu non-local exchange correlation [21] was added. The scalar relativistic wave equation was solved.

The total energy calculations were performed within the ASA in which space is filled with overlapping Wigner-Seitz (WS) atomic spheres. Due to that approximation, several requirements have been fulfilled to minimize the errors in the LMTO method. The symmetry of the potential is considered to be spherical inside each WS sphere. A combined correction takes into account the overlapping part [22]. The values of the atomic sphere radii are chosen in such a way that the sum of all atomic sphere volumes is equal to the volume of the unit cell. Moreover, the radii of the WS spheres for various constituents were obtained by requiring the overlapping potential to be the best possible approximation to the full potential. They were determined by an automatic procedure [22]. The overlap of the WS spheres is approximately 8% for the whole studied concentration of Mn. A volume of the unit cell is set like for the experimental lattice constant [9]. The atomic radii of the WS spheres used in calculations are within the range of 2.6 a.u. to 2.63 a.u. for atoms at an (A,C) site and of 2.66 a.u. to 2.69 a.u. for atoms at B and D sites.

The initial atomic configurations for every atom were taken to be the same as for pure elements. We assumed for Fe: core(Fe) + $3d^64s^2$; for Mn: core(Mn) + $3d^54s^2$; and for Si: core(Si) + $3s^23p^2$. The tetrahedron method [23] was used for integration over the Brillouin zone (BZ). Calculations were carried out for at least 280 k-points in the irreducible wedge of the Brillouin zone. The convergence of the total energy with respect to the number of k-points is attained, when the total energy is stable within 10^{-5} Ry or better.

All electronic structure calculations were carried out using spin-polarised (ferromagnetic) approaches for five values of the x parameter (0, 0.125, 0.25, 0.375, 0.5).

The supercell structure with 32 atoms was used in calculations. It was obtained by the extension into the three dimensional space of the basic positions of DO_3 structure (as in Ref. [19]). Eight positions in the supercell were occupied by silicon atoms (D sites), whereas Fe and Mn atoms occupied the remaining positions (A, B and C). A small disorder effect which was observed experimentally between (A,C) and D sites [13] as well as the disorder between B and D [1,2] were neglected in the present calculations.

The used lattice parameters were the experimental ones as given in reference [9]. The volume of supercell increases almost linearly with manganese content in the investigated range of concentration x ($0 \leq x \leq 0.5$).

3 Site preference

In order to study site preference of Mn in Fe_3Si alloy some of iron atoms in the supercell of the parent compound were substituted by manganese, and total energies of all possible atomic configurations were studied, including also the simultaneous occupation of both (A,C) and B-sites by manganese. Our ab initio total energy calculations of $Fe_{3-x}Mn_xSi$ suggest a site preference of manganese atoms on the B sublattice. This is presented in Table 1, where total energies calculated for different atomic configurations are quoted. The table shows atomic configurations which exhibit minimal energy per atom, E_{min}, and how this energy is raised when Mn atoms occupy other sites.

For the lowest concentration considered ($x = 0.125$) only one iron atom can be substituted by manganese in the supercell. Mn can occupy either a B or an (A,C) position. The total energy of the configuration with one Mn atom located at a B site is approximately 16 mRy/atom lower than for a configuration for which an atom of substitution occurs on an (A,C) site. A similar situation is observed for $x = 0.25$. The most preferable configuration is one for which two Mn atoms are present at B positions. A transfer of one Mn atom to an (A,C) position results in an increase of the total energy by 8 mRy/atom. The third possible configuration, for which two Mn atoms are occupying (A,C) positions, is the least stable arrangement. Its total energy is 54 mRy/atom higher than the minimum energy. For $x = 0.375$ all examined configurations deviating from B site substitution lie at least 28 mRy/atom higher in energy. It is of interest to note that the energies for configurations in 2nd and 3rd columns of the Table 1 are close to each other. Furthermore, for $x = 0.5$ all configurations other than 4Mn(B) substitution exhibit total energies of 155 mRy/atom higher. Moving manganese atoms

Table 1. Results of total energy calculations (per atom). Only deviation from minimal energy values are quoted as a function of x in $Fe_{3-x}Mn_xSi$. The first line indicates configuration of Mn in the supercell, the second gives the total energy relative to the ground state.

x					
0.125	1Mn(B)	1Mn(A,C)			
	E_{min}	E_{min} +16 mRy			
0.25	2Mn(B)	1Mn(B)1,Mn(A,C)	2Mn(A,C)		
	E_{min}	E_{min}+8 mRy	E_{min} + 54 mRy		
0.375	3Mn(B)	2Mn(B),1Mn(A,C)	1Mn(B),2Mn(A,C)	3Mn(A,C)	
	E_{min}	E_{min}+30 mRy	E_{min}+28 mRy	E_{min}+82 mRy	
0.5	4Mn(B)	3Mn(B),1Mn(A,C)	2Mn(B),2Mn(A,C)	1Mn(B),3Mn(A,C)	4Mn(A,C)
	E_{min}	E_{min}+155 mRy	E_{min}+172 mRy	E_{min}+175 mRy	E_{min}+188 mRy

from the B to the (A,C) sublattice increases the total energy by 155 mRy/atom, 172 mRy/atom, 175 mRy/atom and 188 mRy/atom.

Our results are in good agreement with experimental findings [9–11], which indicated a strong B-site preference of manganese for the concentration range considered.

4 Density of states

The spin-projected total densities of states (DOS) calculated in the TB-LMTO method for $Fe_{3-x}Mn_xSi$ (x = 0, 0.125, 0.25, 0.375, 0.5) are presented in Figure 1. The Fermi level is taken as the zero of the energy axis. Presented results refer to the most stable configurations of each $Fe_{3-x}Mn_xSi$ compound. Similar to $Fe_{3-x}Cr_xSi$ [24] and $Fe_{3-x}V_xSi$ [25], a gap is observed in lower energy range in $Fe_{3-x}Mn_xSi$ alloys. This gap (from −0.64 Ry to −0.53 Ry) reflects the large separation of atomic 3s states of silicon from 3p silicon states and states 3d of transition metal elements. Thus, the total DOS consists of two parts. The lower part (below −0.64 Ry) mainly consists of 3s silicon states. In the upper part (above −0.53 Ry) 3d iron states overlap with 3d manganese states for non-zero concentration of doping. With an increase of manganese in Fe_3Si the smearing of some peaks and partial filling of some valleys in the total DOS are observed. The states near Fermi level are mostly of d character with a small p admixture. Furthermore, for the highest concentration considered (x = 0.5) the total DOS strongly changes its shape around Fermi energy. At the Fermi level a new peak appears for the spin-up states. It is formed via the hybridisation of 3d Fe(A,C) and 3d Mn(B) states. Such a pattern can indicate a possible instability for the assumed structure. This can have one of two reasons: the lattice parameter can differ significantly from the lattice parameter obtained from minimum total energy configurations or alternatively for the real system a small deviation of magnetic moments from collinearity can occur. For x = 0.5 we additionally optimised the lattice parameter via the total energy minimalization. The minimum of the total energy for $Fe_{2.5}Mn_{0.5}Si$ is obtained at 10.185 a.u. This value is 4.7% lower than the experimental one [9]. At the theoretical lattice parameter the two changes are revealed in the total DOS. The main peaks of the electronic structure

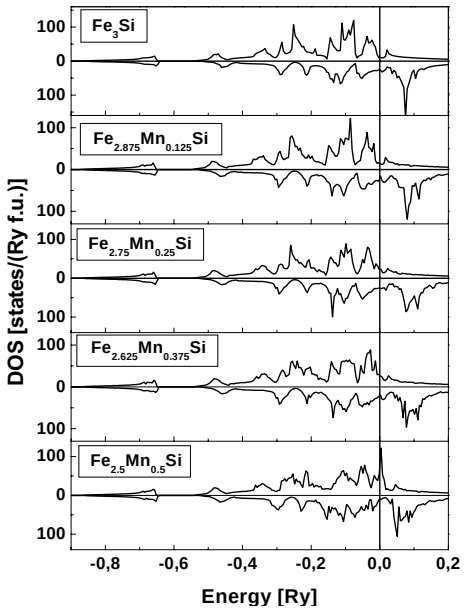

Fig. 1. The spin-projected total density of states for $Fe_{3-x}Mn_xSi$ alloys: Fe_3Si, $Fe_{2.875}Mn_{0.125}Si$, $Fe_{2.75}Mn_{0.25}Si$, $Fe_{2.625}Mn_{0.375}Si$ and $Fe_{2.5}Mn_{0.5}Si$. The vertical line marks the Fermi level.

visibly shift towards lower energy, and the magnitude of these peaks changes. The lower-lying peaks for spin-up direction shift more than peaks located close to the Fermi level. The peak located at the Fermi level remains in the same position (0 Ry). However its magnitude decreases significantly. Thus, the contraction of the supercell can not entirely eliminate this instability. Hence, a magnetic instability is possible for $Fe_{2.5}Mn_{0.5}Si$ due to the high DOS at the Fermi energy.

Figure 2 presents the density of states for Fe(B). Within the whole range of Mn concentrations Fe(B) atoms have the same configuration of the first neighbour shell consisting of 8 Fe(A,C) atoms (manganese atoms can appear only in the third neighbour shell). This local environment is the same as in pure Fe crystallising in the *bcc* structure. As a consequence a similar DOS is obtained [26]. Substitution of Mn on B site does not change the position of the main peaks of Fe(B). This result can be associated

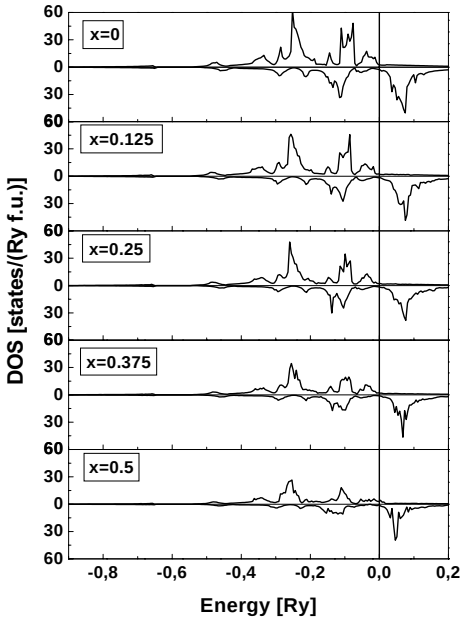

Fig. 2. The spin-projected density of states for Fe in B position for $Fe_{3-x}Mn_xSi$ alloys: Fe_3Si, $Fe_{2.875}Mn_{0.125}Si$, $Fe_{2.75}Mn_{0.25}Si$, $Fe_{2.625}Mn_{0.375}Si$ and $Fe_{2.5}Mn_{0.5}Si$.

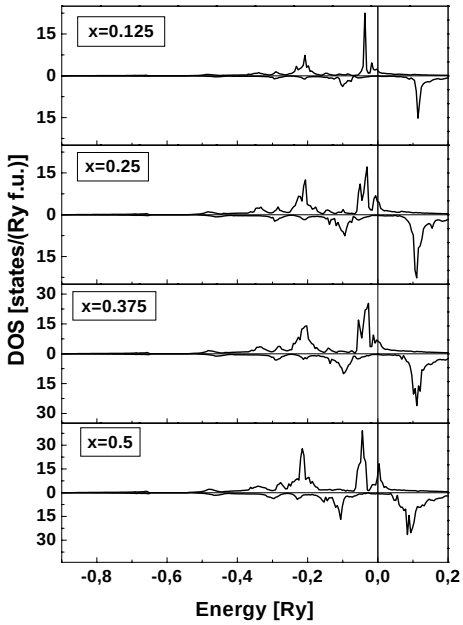

Fig. 3. The spin-projected density of states for Mn in B position for $Fe_{3-x}Mn_xSi$ alloys: $Fe_{2.875}Mn_{0.125}Si$, $Fe_{2.75}Mn_{0.25}Si$, $Fe_{2.625}Mn_{0.375}Si$ and $Fe_{2.5}Mn_{0.5}Si$.

with a partial screening of the impurity Mn atom by its first nearest neighbours. The drop of the intensity of the main peaks of Fe(B) with concentration x, which is observed in the DOS picture somewhat below the Fermi energy, is connected with a decrease of the number of iron atoms on B positions. Manganese atoms on B positions have the same nearest neighbours surrounding as Fe(B) atom. The calculated DOS of Mn(B) (Fig. 3) reveals the same features as the electronic structure of Mn atoms in other Mn-based Heusler alloys with $L2_1$-structure [27]. Due to a large exchange splitting of Mn $3d$ states, the typical separation of bonding and antibonding electronic states is observed in the local DOS of Mn(B). Thus, below Fermi energy the number of states for spin-up direction is much higher than the number of states for spin-down. This is demonstrated by the large magnetic moment of manganese oriented parallel to the magnetic moment of iron. It is interesting to note that the highly occupied electronic states of Mn are located close to the Fermi level (E_F). This yields a high total DOS at the E_F.

The total electronic density of states $N(E_F)$ increases with Mn concentration. Thus, an increase of the electronic specific-heat is expected for Fe_3Si doped with Mn atoms. Using the result of the presented calculations we estimated the value of the electronic specific-heat coefficient using the relation:

$$\gamma = \frac{\pi^2 k_B^2}{3} N(E_F), \qquad (1)$$

where k_B is the Boltzmann constant, $N(E_F)$ is the total electronic density of states for experimental lattice parameters. The electronic specific-heat coefficient and the experimental value of lattice parameter are listed in Table 2. The value of $\gamma_{theor} = 10.68$ mJ/(mol K^2) for $x = 0.5$ corresponds to the sharp DOS spike at the Fermi level for

Table 2. Electronic specific-heat coefficient γ in [mJ/(mol K^2)] for $Fe_{3-x}Mn_xSi$.

x	a_{exp} [a.u.]	γ_{theor}
0	10.6829	6.44
0.125	10.6851	6.56
0.25	10.6872	7.88
0.375	10.6893	7.64
0.5	10.6915	10.68

spin-up electronic states of Mn(B) and of Fe(A,C). Indeed, some experimental results have shown evidence of antiferromagnetic ordering in $Fe_{3-x}Mn_xSi$ for a somewhat higher concentration of Mn [1,28,29]. This allows us also to consider a noncollinear alignment for $x = 0.5$.

The nearest neighbour shell of Fe(A,C) in Fe_3Si is formed by two types of atoms: four silicon and four iron atoms. At higher concentrations some manganese atoms can be found in the surrounding of Fe(A,C). All this yields much more structured DOS. Atomic $3d$-levels of Fe(A,C) (Fig. 4) are much less distinct than for Fe(B) (Fig. 2) and Mn(B) (Fig. 3). With increasing manganese content the difference decreases between spin-up and spin-down states below Fermi energy. This is reflected in a decreasing magnetic moment of Fe(A,C) with manganese doping. For the highest concentration a strong peak for the majority DOS and a significant decrease of the density of states for minority carriers appears at the Fermi level. Something like a pseudogap, slightly above the Fermi energy, is formed. In order to shed more light on this issue the densities of states of Fe in (A,C) position with a different local neighbourhood for $Fe_{2.5}Mn_{0.5}Si$ are presented in Figure 5. The strong influence of neighbouring manganese atoms on the

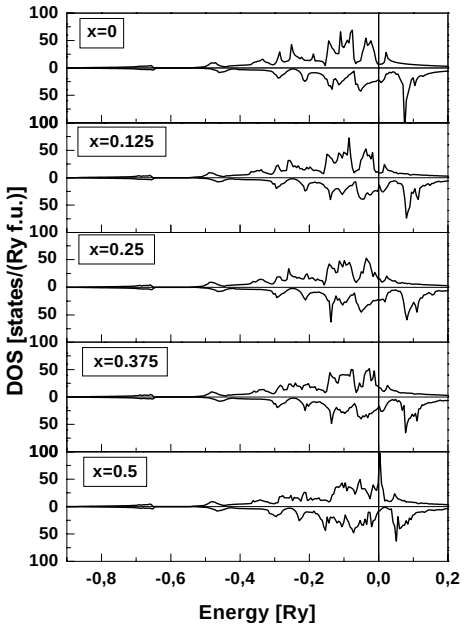

Fig. 4. The spin-projected density of states for Fe in (A,C) position for $Fe_{3-x}Mn_xSi$ alloys: Fe_3Si, $Fe_{2.875}Mn_{0.125}Si$, $Fe_{2.75}Mn_{0.25}Si$, $Fe_{2.625}Mn_{0.375}Si$ and $Fe_{2.5}Mn_{0.5}Si$.

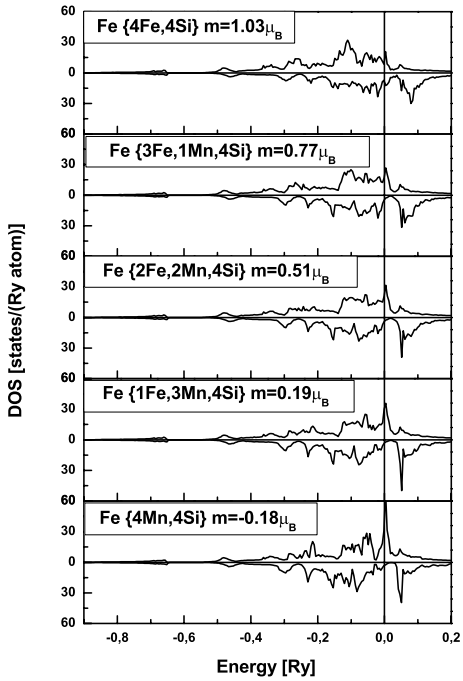

Fig. 5. The spin-projected density of states for Fe in (A,C) position for $Fe_{2.5}Mn_{0.5}Si$ for different local environment configurations. There are given in brackets configurations of 1NN, m means local magnetic moment.

iron density of states is seen. For the configuration of the nearest shell consisting of only iron and silicon atoms, a small peak is present for the majority DOS of Fe(A,C) at the Fermi level. With increasing manganese content in the nearest neighbour shell, a strong increase of this peak is observed. This arises due to hybridisation of $3d$ states of iron on (A,C) positions with $3d$ states of manganese at the Fermi level.

Local densities of states of silicon are shown in Figure 6. In all alloys studied here Si atoms are located at D positions. They are surrounded by 8 Fe(A,C) atoms. Manganese atoms can appear only within the third neighbour shell of silicon. Therefore the influence of the Mn concentration on the silicon electronic states is small. A complete separation of states below -0.64 Ry from electronic states with energies above -0.53 Ry is visible in the silicon DOS picture. The lower energy part of this DOS is formed almost uniquely by $3s$ spherical states, whereas the higher energy part consists mainly of $3p$ states. They exhibit asymmetry for spin-up and spin-down directions. The peak at -0.29 Ry in the minority subband of Si, which is derived from p-states, still remains at the same position irrespective of the concentration of Mn.

5 Magnetic moments

The results of the self-consistent electronic structure calculations allow for a detailed analysis of both, the total and the local magnetic moments in $Fe_{3-x}Mn_xSi$. The magnetic moment on Fe atoms strongly depends on the site occupied by the atom in the unit cell and on the configuration of the nearest neighbours. A much weaker dependence of the total magnetic moment on the concentration of manganese is observed. In the following discussion we concentrate mainly on values of the magnetic moment for configurations with the smallest total energy.

Because of the different local environment of B and (A,C) positions, a different behaviour is expected of magnetic moments of atoms at these sites. It was reported by Yoon [3] that the magnetic moment on B sites is approximately constant up to a concentration of $x = 0.75$. In contrast, the magnetic moment observed on (A,C) positions is claimed to decrease linearly to a value of $0.4\mu_B$ for $x = 0.75$. A similar behaviour of the iron magnetic moment is obtained in our study (Fig. 7).

For pure Fe_3Si compound the values of the magnetic moments of Fe(A,C) and Fe(B) are equal to $1.42\mu_B$ and $2.62\mu_B$, respectively. They are higher by about $0.2\mu_B$ than the moments determined using various experimental techniques [14,15]. This may be explained by two effects. Firstly, we neglect in our calculations partial disorder between D and B as well as D and (A,C) positions. Secondly, experiments were carried out at non-zero absolute temperature, while our calculations correspond to 0 K.

With doping the average magnetic moment of iron slightly increases to a value of $2.72\mu_B$ for the highest concentration considered (Fig. 7). Similar behaviour was obtained in $Fe_{3-x}V_xSi$ [25], where the vanadium moment antiferromagnetically orientated with respect to the Fe moment. When manganese atoms locate within the nearest neighbour shell it causes, according to our calculations, a decrease of magnetic moment of iron. However the presence of one manganese atom only within the third

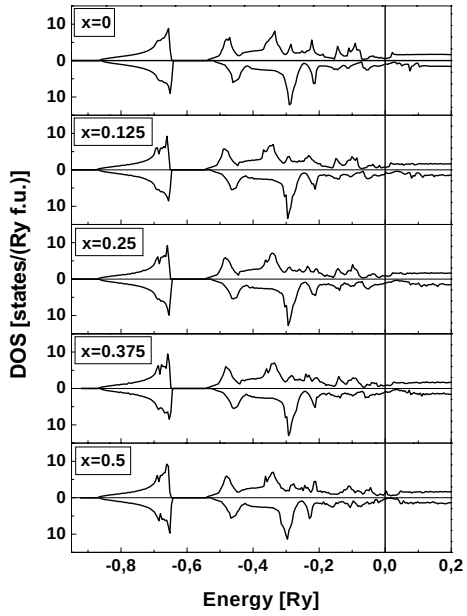

Fig. 6. The spin-projected density of states for Si in D position for $Fe_{3-x}Mn_xSi$ alloys: Fe_3Si, $Fe_{2.875}Mn_{0.125}Si$, $Fe_{2.75}Mn_{0.25}Si$, $Fe_{2.625}Mn_{0.375}Si$ and $Fe_{2.5}Mn_{0.5}Si$.

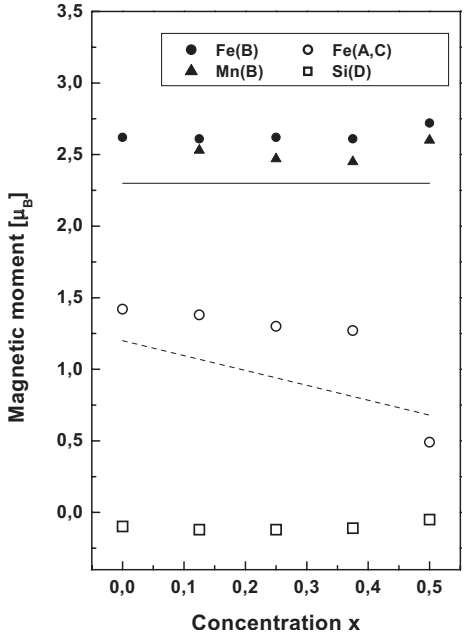

Fig. 7. The dependence of the average magnetic moments on the concentration x for $Fe_{3-x}Mn_xSi$ alloys. The solid and dashed lines correspond to the results [9] of magnetic moments on B site and on (A,C) site, respectively.

neighbour shell leads to a marginal increase of the magnetic moment of iron by about $0.01\mu_B$.

For the highest concentration the minimum energy was obtained for a configuration with Fe(B) having 6 manganese neighbours in the third shell. In all these cases the iron atoms are having only iron atoms as the first nearest neighbours. If configurations with higher total energies are taken into account, we obtained result where iron atoms at B position with the 3NN=8Mn,4Fe exhibit magnetic moment equal to $2.75\mu_B$. This indicates that this magnetic moment does not much depend on the Mn concentration within the 3rd n.n. shell.

An apparent decrease of the value of the Fe (A,C) moment with concentration x is a consequence of the first nearest neighbour shell of the iron atom. The magnetic moments of Fe(A,C) vary significantly depending on the chemical environment. Manganese atoms can locate within the first shell around Fe(A,C). A variety of different atomic configurations of the local environment can be obtained. This explains the rather sudden drop of the magnetic moment at $x = 0.5$. The average magnetic moment of Fe(A,C) decreases nonlinearly from its value of $1.42\mu_B$ for pure Fe_3Si compound to $0.49\mu_B$ for $Fe_{2.5}Mn_{0.5}Si$ alloy. The overall decrease is produced mainly by manganese atoms located within the nearest neighbour shell. Each additional Mn atom substituting for Fe(B) causes the decrease of the magnetic moment of Fe(A,C) by about $0.2\mu_B$. The experimentally observed value of $0.34\mu_B$ [11,30] is higher than the calculated one. For the concentration of $x = 0.5$ the local magnetic moment of Fe changes drastically from $1.03\mu_B$ when 1NN=4Fe(B),4Si(D) to $-0.18\mu_B$ when only manganese and silicon atoms (1NN=4Mn,4Si) are found in the first neighbour shell. The reversal of the direction of the Fe magnetic moment with respect to the total magnetic moment is similar to $Fe_{3-x}Cr_xSi$ with $x = 0.5$ and 1NN=4Cr,4Si [31]. This indicates the possibility of a non-collinear configuration of magnetic moments. For the same configuration of local environment (1NN=4Mn, 4Si) Kepa et al. assigned $0\mu_B$ magnetic moment of Fe [12]. This agrees rather well with our results. The difference can be explained by the fact the experiment [12] has been conducted at room temperature. We note, however, that this experiment was carried out on a sample with Mn concentration below $x = 0.5$. Furthermore, the calculated rapid drop of Fe(A,C) magnetic moment for $x = 0.5$ is produced mainly by spin reorientation when first neighbour shell is formed by 4 Mn and 4 Si atoms. Therefore the observed differences between experimental and theoretical value may well be explained by the clustering of manganese atoms in the supercell. This was indeed observed in neutron diffuse scattering experiments for even lower Mn concentrations [12,30]. Because of the limitation of the procedure applied here, such effects can not be included into the calculation scheme.

The magnetic moment of manganese at B positions is oriented parallel to the total magnetic moment as in $Fe_{3-x}Mn_xAl$ [32]. Values of the magnetic moment of Mn change within the range of $2.45\mu_B$ to $2.60\mu_B$. Similarly as for the iron atom, the presence of Mn in the third neighbour shell substituting for iron atoms causes an increase of magnetic moment of manganese. The lowest value ($2.45\mu_B$) corresponds to the atomic configuration 1NN=8Fe, 2NN=6Si, 3NN=12Fe, whereas the highest value ($2.60\mu_B$) is obtained for Mn atom with the following local environment: 1NN=8Fe, 2NN=6Si, 3NN=6Fe,6Mn. The values of the manganese magnetic moment obtained

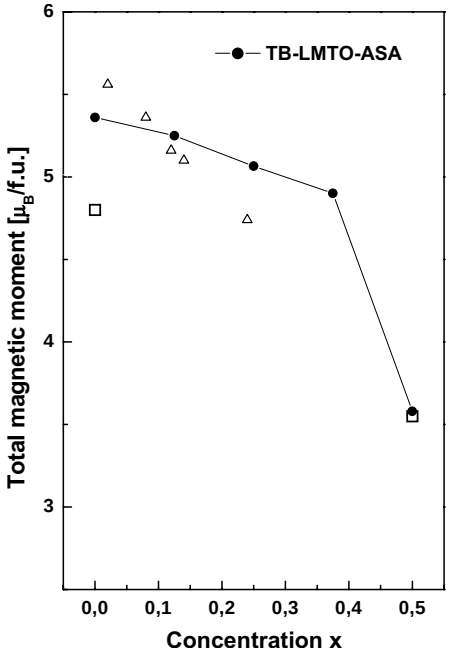

Fig. 8. The dependence of the total magnetic moment on the concentration x for $Fe_{3-x}Mn_xSi$ alloys. The values of the magnetic moment are marked as squares and as triangles corresponding to the experimental results of references [3,15], respectively.

theoretically are about $0.2\mu_B$ higher than the values determined from neutron diffraction [29] and NMR data [3].

Within the whole concentration a small negative moment on silicon is present. A similar result was obtained earlier for $Fe_{3-x}Cr_xSi$ [24]. Small negative polarisation of silicon atoms was postulated also by Moss and Brown [33] and by Dobrzyński [34].

Figure 8 presents the concentration dependence of the total magnetic moment. The values presented concern configurations with the lowest total energies. The value of total magnetic moment visibly decreases from $5.36\mu_B$ for Fe_3Si to $3.58\mu_B$ in case of $Fe_{2.5}Mn_{0.5}Si$. The change of the magnetic moment with the concentration is mainly determined by the decrease of the magnetic moment on iron atoms in (A,C) positions, which is in qualitative agreement with the experimental data [11,15]. We note, however, that the experimental slope of the magnetisation obtained from saturation magnetisation measurements [15] is higher than theoretical one. This can be due to the fact that the calculations did not take either partial disorder between sublattices or short-range order into account.

6 Conclusions

Within the range of concentrations $0 < x \leq 0.5$ $Fe_{3-x}Mn_xSi$ fulfils the rule of selective location of Mn atoms in non-equivalent positions [8–10]. The calculations indicate a strong B site preference of manganese. Furthermore, the difference between the total energy of the most preferable configuration and the total energies of other configurations increases with concentration. One can conclude that within the studied concentration range no indications are found of a tendency of Mn to occupy (A,C) sites as observed experimentally for $x > 0.75$ [11].

The atomic magnetic moments and the densities of states are obtained for the two non-equivalent positions. The densities of states of Fe(B) resemble the DOS of Fe in the *bcc* structure because of an identical configuration of the nearest neighbour shell. Our results indicate that the magnetic moment of iron depends on the position which atoms occupies and on the local environment. Manganese atoms located in the 1NN cause a decrease of magnetic moments on iron atoms. While the magnetic moment of Fe(A,C) is sensitive to the atomic configuration of the nearest neighbour shell, the magnetic moment of Fe(B) remains almost constant within the whole range of concentration. The magnetic moment of manganese is oriented parallel to the magnetic moment of iron atoms. The presence of manganese atom in the nearest neighbour shell causes a decrease of an iron magnetic moment, whereas manganese atom in the third shell leads to a small and opposite effect. A small negative magnetic moment is induced on the silicon atoms. The total magnetic moment decreases with increasing Mn concentration. The observed differences between experimental and theoretical rates of drop can be attributed to the clustering of Mn atoms reported in [12].

References

1. J.T.T. Kumaran, C. Bansal, Solid State Commun. **69**, 779 (1989)
2. L. Dobrzyński, J. Phys.: Condens. Matter. **7**, 1373 (1995)
3. S. Yoon, J.G. Booth, Phys. Lett. A **48**, 381 (1974)
4. A. Paoletti, L. Passari, Nuovo Cim. **32**, 25 (1964)
5. G.D. Mukherejee, C. Bansal, A. Chatterjee, Physica B **254**, 223 (1998)
6. H. Miki, K. Ohoyama, H. Onodera, Y. Yamauchi, Y. Yamaguchi, H. Nojiri, M. Motokawa, S. Funahashi, S. Tomiyoshi, Physica B **237–238**, 465 (1997)
7. S. Bednarski, K. Siemensmeyer, M. Slepowronski, E. Garcia-Matres, M. Winkelmann, Physica B **234–236**, 1074 (1997)
8. T.J. Burch, T. Litrenta, J.I. Budnick, Phys. Rev. Lett. **33**, 421 (1974)
9. V. Niculescu, K. Raj, T.J. Burch, J.I. Budnick, Phys. Rev. B **13**, 3167 (1976)
10. T.J. Burch, J.I. Budnick, V. Niculescu, K. Raj, T. Litrenta, Phys. Rev. B **24**, 3866 (1981)
11. S. Yoon, J.G. Booth, J. Phys. F: Metal. Phys. **7**, 1079 (1977)
12. H. Kepa, T.J. Hicks, R.L. Davis, Mat. Sci. For. **27/28**, 267 (1988)
13. G.A. Al-Nawashi, S.H. Mahmood, A.F.D. Lehloch, A.S. Saleh, Physica B **321**, 167 (2002)
14. J. Waliszewski, L. Dobrzyński, A. Malinowski, D. Satuła, K. Szymański, W. Prandl, Th. Brückel, O. Schärpf, J. Magn. Magn. Mater. **132**, 349 (1994)
15. W.A. Hines, A.H. Menotti, J.I. Budnick, T.J. Burch, T. Litrenta, V. Niculescu, K. Raj, Phys. Rev. B **13**, 4060 (1976)

16. D.E. Eastman, J.F. Janak, A.R. Williams, R.V. Coleman, G. Wendin, J. Appl. Phys. **50**, 7423 (1979)
17. E.J.D. Garba, R. Jacobs, J. Phys. F **16**, 1485 (1986)
18. Y. Yamagushi, T.R. Thurston, H. Miki, S. Tomiyoshi, Physica B **213**, 363 (1995)
19. O.K. Andersen, O. Jepsen, M. Sob, *Electronic Structure and Its Applications*, edited by M. Yuassoff (Springer-Verlag, Berlin, 1987), p. 2
20. U. von Barth, L. Hedin, J. Phys. C **5**, 1629 (1972)
21. C.D. Hu, D.C. Langreth, Phys. Scr. **32**, 391 (1985)
22. O. Jepsen, O.K. Andersen, Z. Phys. B **97**, 645 (1995)
23. O. Jepsen, O.K. Andersen, Solid State Commun. **9**, 1763 (1971)
24. M. Pugaczowa-Michalska, A. Go, L. Dobrzyński, S. Lipiński, J. Magn. Magn. Mater. **256**, 46 (2003)
25. A. Bansil, S. Kaprzyk, P.E. Mijnarends, J. Toboła, Phys. Rev. B **60**, 13396 (1999)
26. J. Kübler, O.K. Andersen, O. Jepsen, M. Sob, *Theory of Itinerant Electron Magnetism* (Oxford, 2000), p. 235
27. S. Plogmann, T. Schlathölter, J. Braun, M. Neumann, Yu.M. Yarmoshenko, M.V. Yablonskikh, E.I. Shreder, E.Z. Kurmaev, A. Wrona, A. Ślebarski, Phys. Rev. B **60**, 6428 (1999)
28. T. Ersez, G.T. Etheridge T.J. Hicks, J. Magn. Magn. Mater. **177–181**, 1351 (1998)
29. V. Niculescu, T.J. Burch, J.I. Budnick, J. Magn. Magn. Mater. **39**, 223 (1983)
30. K. Kepa, T.J. Hicks, J. Phys. C **8**, 111 (1988)
31. A. Go, M. Pugaczowa-Michalska, L. Dobrzyński, J. Magn. Magn. Mater. **272–276**, e217 (2004)
32. M. Pugaczowa-Michalska, A. Go, L. Dobrzyński, Phys. Stat. Sol. b **242**, 463 (2005)
33. J. Moss, P.J. Brown, J. Phys. F: Met. Phys. **2**, 358 (1972)
34. L. Dobrzyński, J. Phys.: Condens. Matter **7**, 1373 (1995)